Geotextiles and Geomembranes 11 (1992) 185–219

Short-Term Strength and Deformation Characteristics of Geotextiles Under Typical Operational Conditions

Hoe Ing Ling

Department of Civil Engineering, University of Tokyo, 7-22-1 Ropponggi, Minato-ku, Tokyo 106, Japan

Jonathan T. H. Wu

Department of Civil Engineering, University of Colorado at Denver, Denver, Colorado 80204, USA

&

Fumio Tatsuoka

Institute of Industrial Science, University of Tokyo, 7-22-1 Ropponggi, Minato-ku, Tokyo 106, Japan

(Received 4 December 1990; accepted 25 January 1991)

ABSTRACT

An apparatus capable of measuring the strength and deformation properties of geotextiles under unconfined conditions and under the confinement of a membrane or a soil was developed. The appratus differed from conventional in-soil test apparatuses in that during the soil-confinement test the soil was allowed to deform with the geotextile while being confined by a prescribed pressure — simulating the predominant operational condition of geotextiles in reinforced soil structures. Three non-woven geotextiles manufactured in different materials and by different bonding processes were used in this study, and their stress-confinement effects were studied. It was shown that the stress-confinement effect existed in the spun-bonded and needle-punched geotextiles but not in the heat-bonded geotextile. The effect of using different materials (membrane and soil) for the confinement was also studied. Under otherwise identical conditions, the results were very similar between the in-membrane

Geotextiles and Geomembranes 0266–1144/92/$03.50

and in-soil tests. It was concluded that the in-membrane test is sufficient for evaluating the load–deformation properties of geotextiles. Mathematical models were used to represent the measured load–deformation relationships of the geotextiles, and their accuracy was discussed.

NOTATION

a, b	Parameters for the hyperbolic model
$a_1, a_2, \ldots$	Polynomial constants
E_i	Initial tensile modulus
E_{sec}	Secant modulus
T	Load per unit width
T_f	Load per unit width at failure
W/L	Width to length ratio (aspect ratio)
y, z	Constants relating initial tensile modulus to effective normal stress
y', z'	Constants relating failure load to effective normal stress
ε	Axial tensile strain
ε_f	Strain at failure (failure strain)
σ_n'	Effective normal stress

1 INTRODUCTION

Due to the increasing popularity of geotextile-reinforced soil structures in earthwork construction, various procedures for the analysis and design of such structures have been proposed. Current analytical procedures are based on either the limit equilibrium method or the finite element method. The former evaluates the internal and external stability of the structures, whereas the latter computes their deformations and the stress distribution in the structures. For analysis by the finite element method, it is generally required to supply the deformation parameter of the geotextile for a linear elastic model, and the deformation and strength parameters for a non-linear elastic or elastoplastic model. The exact required parameters, however, depend on the individual models used. These parameters should be supplied in a manner simulating the operational condition of the geotextile-reinforced soil structures. In the limit equilibrium analysis, since only the ultimate state of a geotextile is of interest, the strength of the geotextile serves as the main parameter for the analysis. The design strength is based on the failure strength or the

strength mobilized at a selected value of strain level, for example, that at 10% strain.

When the deformation and strength properties of a geotextile are determined in the laboratory, they should be measured in a manner which best replicates the predominant operational condition of the geotextile in the field. However, some methods of testing, for example, the grab method (ASTM, 1987*a*) and the strip method (ASTM, 1987*b*) are based on those of the textile industry and the results obtained can only be considered index properties. Some researchers (El-Fermaoui & Nowatzki, 1982; Siel *et al.*, 1987; Wu & Su, 1987; Juran & Christopher, 1989) have suggested that the tensile characteristics of geotextiles should be measured under the soil-confinement condition. The modified shear box and the pullout box have been used in which the geotextile was embedded between upper and lower boxes and stressed up to failure. McGown *et al.* (1981, 1982) developed a more sophisticated apparatus, as shown in Fig. 1, for measuring the tensile properties of geotextiles under soil-confinement condition. In this apparatus, a geotextile specimen was confined with soil on both sides using air pressure bellows enclosed in two metal boxes. This research triggered a series of studies on the confined tensile properties of geotextiles. For example, Nishigata & Yamaoka (1989) constructed a similar apparatus and Kokkalis & Papacharisis (1989) modified a direct shear apparatus in a simplified version. Furthermore, Christopher *et al.* (1986) also developed a zero span confined test and compared their results with those of McGown *et al.*

One of the important findings derived from these in-soil tests was that there was a significant increase in the stiffness and strength of the geotextiles confined with soil compared with the unconfined condition. However, it is very likely that these in-soil tests did not simulate the operational conditions of a geotextile in a reinforced soil structure, because in these tests the soil was kept stationary inside a box, and the geotextile had to overcome the frictional resistance against the stationary soil before the tensile load in the geotextile could be mobilized. As a result, the measured load reflects the combined effects of the frictional force and the stress confinement. In geotextile-reinforced soil structures under typical operational conditions, slippage at the soil–geotextile interfaces will not occur until a failure state is approached. Therefore, these apparatuses would overestimate the strength and stiffness of extensible geotextiles and might render the design unsafe. Besides, the laboratory testing always aims to measure the material properties of geotextile and the tests are to be performed under conditions with a

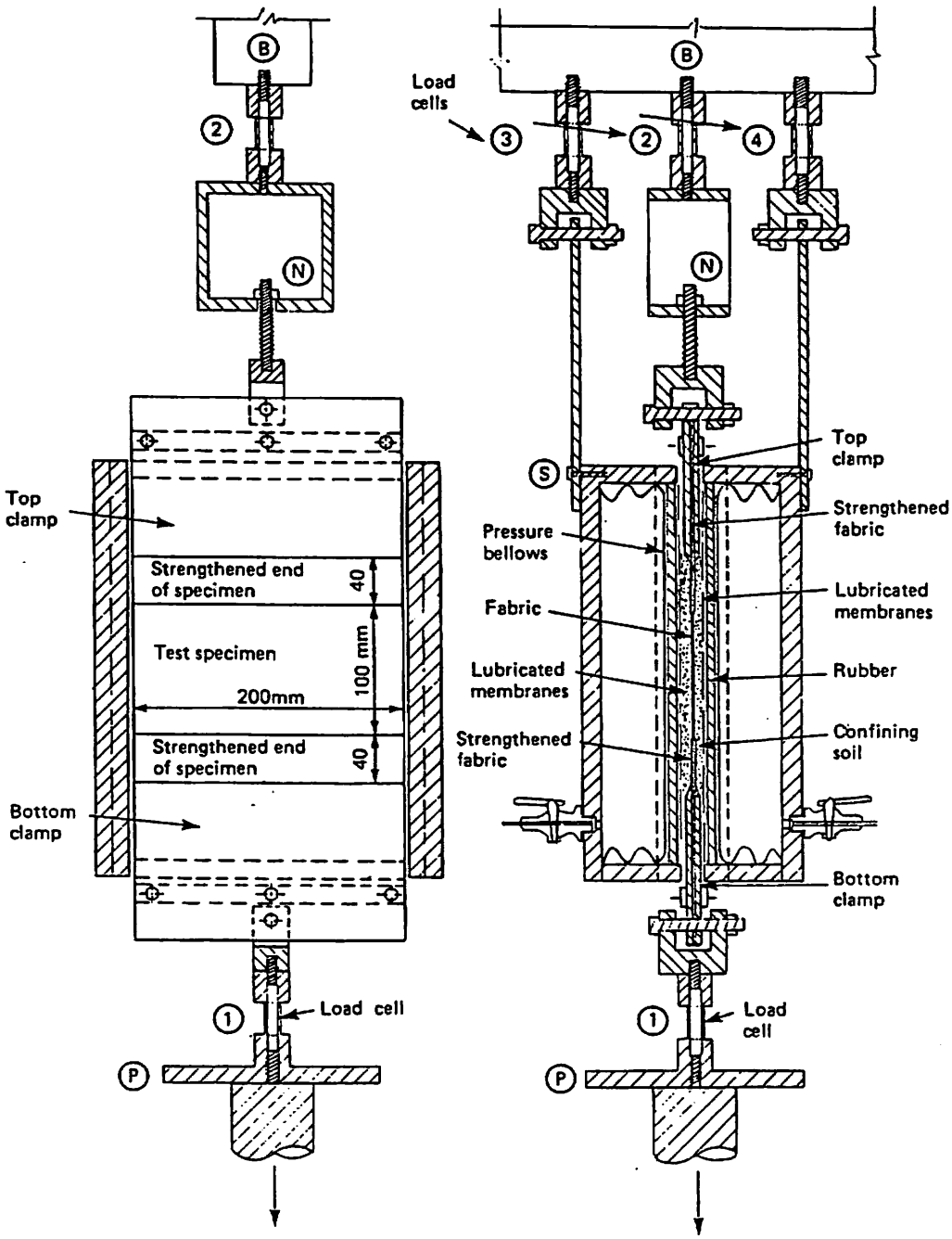

Fig. 1. An in-soil test apparatus (McGown *et al.*, 1981).

minimum boundary effect. Because of this, the conventional in-soil tests should be considered to be model tests in which due to the frictional force, the strain and tensile load were not only non-uniform along the length of the specimen but also sensitive to the boundary conditions; hence the test results were difficult to interpret correctly. A more detailed discussion is given by Wu (in press).

In view of the above, other methods for measuring the confined stiffness and strength of geotextiles were developed by Tatsuoka *et al.* (1985), Tatsuoka & Yamauchi (1986) and Wu & Arabian (1990). Tatsuoka and co-workers used two cylindrical membranes to confine a geotextile sewn into a cylindrical sleeve, as shown in Fig. 2, in which air pressure was used to confine the geotextile. The effect of stress confinement was studied by assuming that the use of soil would not induce additional confinement effects. Wu & Arabian developed a cylindrical testing apparatus, as shown in Fig. 3, in which the geotextile was confined by a cylindrical soil column of diameter 15·24 cm. In this method, the soil was allowed to deform in the axial direction with the geotextile which allowed the inherent load-deformation properties of geotextiles under soil confinement to be determined.

A direct comparison between the results of in-membrane and in-soil tests is lacking. Tatsuoka *et al.* performed tests with the geotextile confined by the membrane only and Wu & Arabian performed tests on the geotextile confined by a soil column only. In addition, the apparatus used by Tatsuoka *et al.* was too sophisticated and suffered from

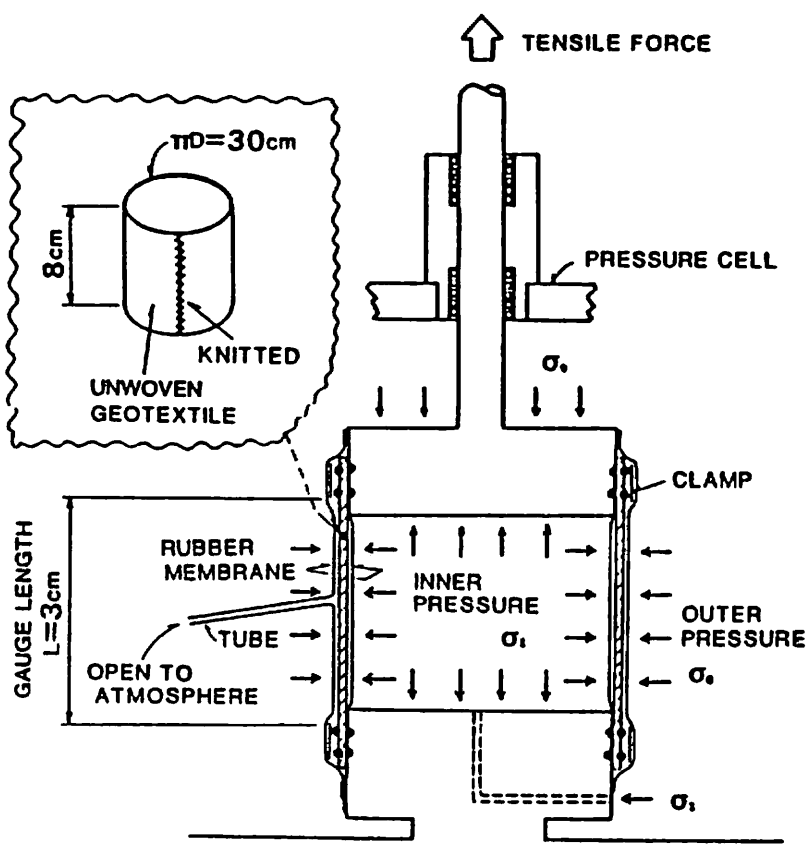

Fig. 2. An in-membrane test apparatus (Tatsuoka *et al.*, 1986).

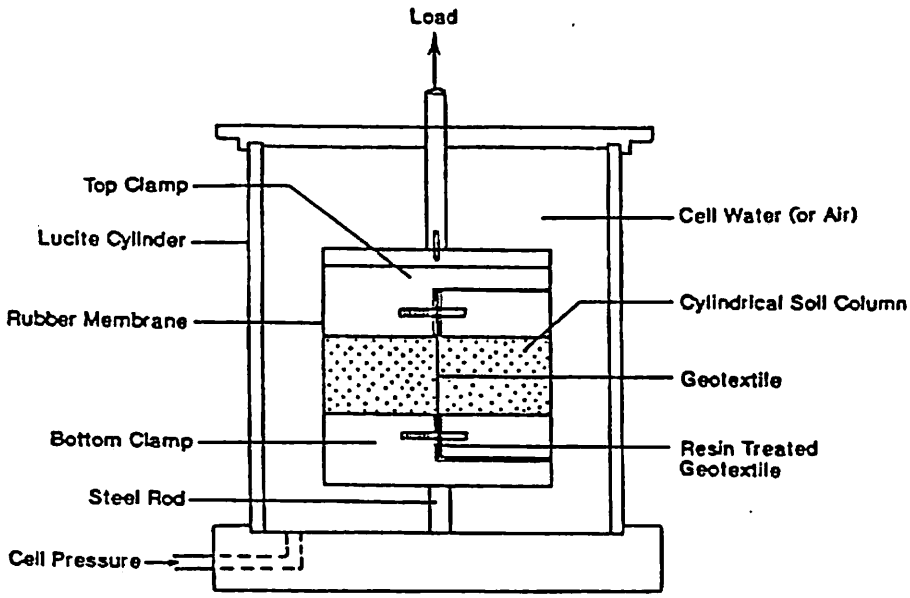

Fig. 3. The cylindrical test apparatus (Wu & Arabian, 1990).

difficulties with providing a strong seam and an effective clamping system, as the deformation may be concentrated at the seam and near the clamp when a high-strength geotextile is tested. Wu & Arabian, on the other hand, used a relatively large diameter soil column to confine the geotextile which could produce a relatively large triaxial extension resistance from the soil and needed to be subtracted from the measured load. This may lead to some degree of uncertainty in the results because:

(i) The triaxial extension strength of soil has been known to be sensitive to the failure mode, which is controlled by the dimensions of the specimen and the boundary conditions. For example, Lam & Tatsuoka (1988) have shown that the triaxial extension strength of sand for the conventional specimen dimension of a height/diameter ratio of 2 was much smaller due to the necking failure mode when compared to that for a squat (more disk-like) specimen which did not exhibit the necking failure mode.

(ii) The triaxial extension strength of soil alone in the case of the test shown in Fig. 3 may also be influenced by the presence of a geotextile in addition to its specific dimensions, and thus may be difficult to evaluate.

In the present study, an apparatus has been developed to measure the confined and unconfined tensile properties of geotextiles. Three non-woven geotextiles manufactured by different processes and materials were tested in this study. The effect of stress confinement on the three

geotextiles was investigated. Two methods of stress confinement, with a soil and with a rubber membrane, were examined. In addition, mathematical representation of the test results was presented and discussed.

2 TESTING APPARATUS AND TESTING PROCEDURE

The apparatus shown in Fig. 4a was designed to measure the strength and deformation properties of a geotextile under unconfined conditions (in-air test), under the confinement of a rubber membrane (in-membrane test) and under the confinement of a soil (in-soil test). The apparatus comprises two sets of clamps configured to accommodate two thin cubical-shaped soil cakes enclosed in a rubber membrane to confine the geotextile specimen (in the in-soil test). The configurations of the in-air, in-membrane and in-soil tests are shown, respectively, in Fig. 5(a), (b) and (c).

The clamps allowed a maximum width of geotextile specimen up to 30 cm to be tested, as shown in Fig. 4b. Varying values of length of the geotextile specimen may be selected to obtain different values of aspect ratio (width/length, W/L). Furthermore, geotextiles of different thicknesses could be tested by adjusting the jaws sideways.

The clamps were connected to a loading mechanism by two circular rods. The lower rod, the length of which can be varied according to the length of geotextile desired, was fixed to the bottom of the loading frame. Tensile loads were applied to the geotextile specimen at a constant rate of displacement through the upper rod as in the conventional triaxial extension test of soil. The elongation of the geotextile was obtained by measuring the displacement of the upper rod with two displacement transducers. For the results shown in this paper, a transducer having a capacity of 4 cm was used to measure small strains; for strains up to failure the other transducer, with a capacity of 20 cm, was employed. Besides the load and the displacement measurements, a partial vacuum (suction) applied to the geotextile was measured in the case of the in-membrane and in-soil tests. All the measurements were taken at a regular time interval and then converted from analog to digital signals before being recorded by a personal computer.

3 TEST MATERIALS

Three types of non-woven geotextile, Bidim b5, Tafnel R-90k, and Typar 3301, each manufactured by a different bonding process, were selected

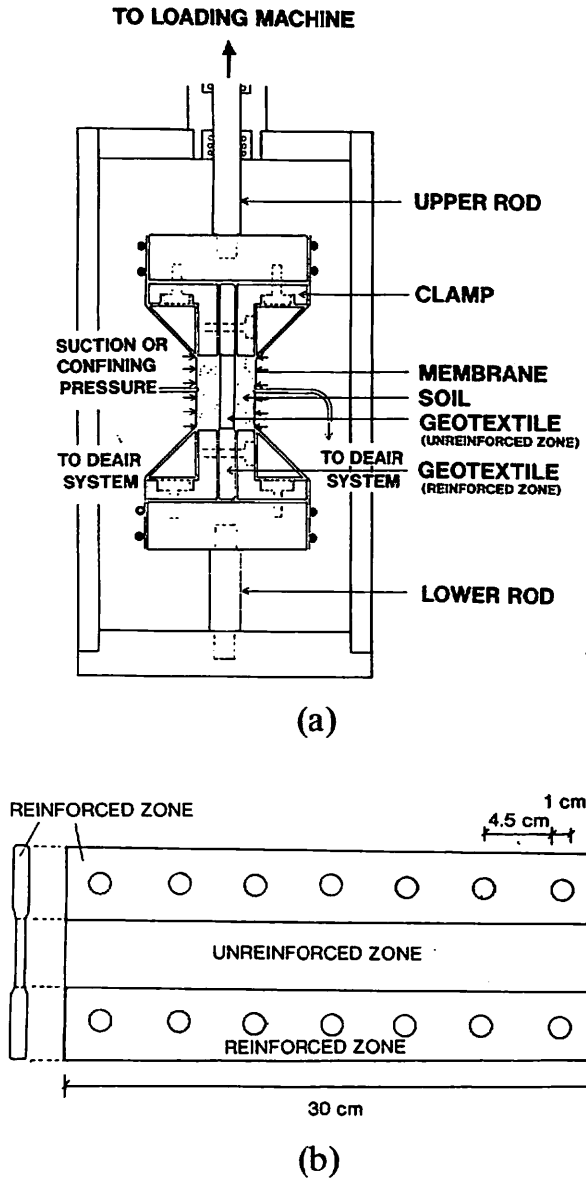

Fig. 4. (a) The in-soil test apparatus, (b) configuration of geotextile specimen.

for this study. In the subsequent sections, they are referred to as the spun-bonded geotextile, the needle-punched geotextile, and the heat-bonded geotextile, respectively. The fiber of the spun-bonded and heat-bonded geotextiles was manufactured from polypropylene and the needle-punched geotextile fiber was manufactured from polyester. The mass per unit area and unstressed nominal thickness of these three geotextiles are given in Table 1.

The soil used in the in-soil tests was Toyoura sand, the strength and deformation characteristics of which have been studied in detail elsewhere (Tatsuoka *et al.*, 1986; Lam & Tatsuoka, 1988). It is a fine

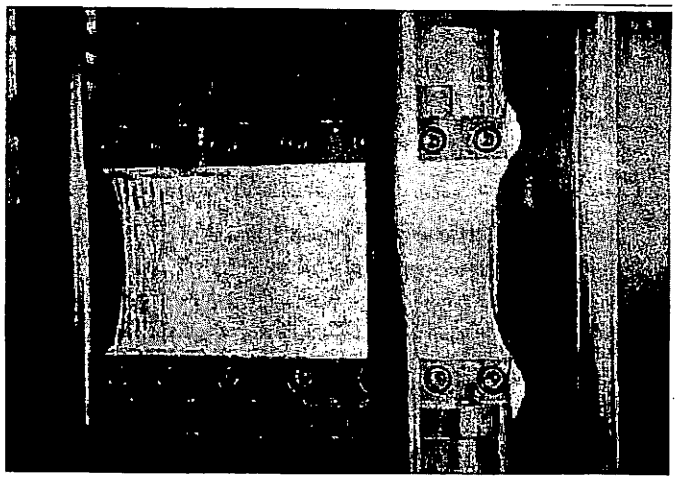

(a)

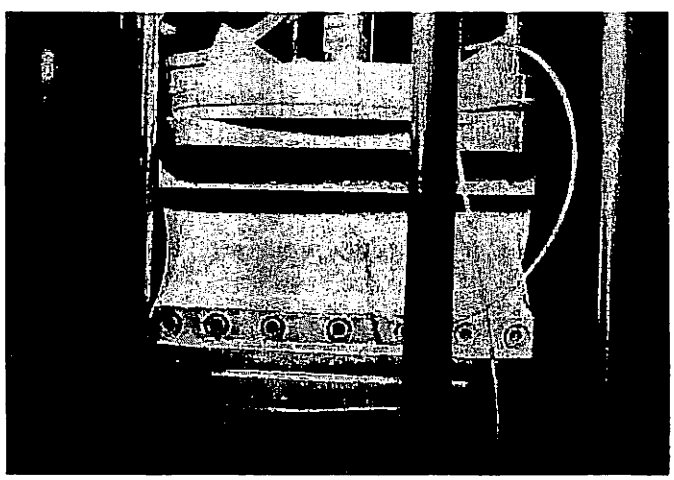

(b)

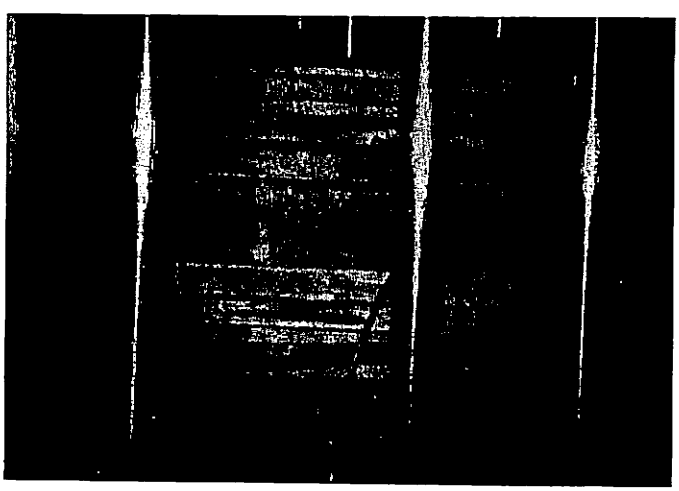

(c)

Fig. 5. Tests in progress: (a) in-air test, (b) in-membrane test, (c) in-soil test.

Table 1
Index Properties of Geotextiles

Geotextile	*Bonding process*	*Polymer type*	*Mass per unit area (g/m^2)*	*Thickness (mm)*
Bidim b5	Needle-punched	Polyester	235	3
Tafnel R-90k	Spun-bonded	Polypropylene	300	3
Typar 3301	Heat-bonded	Polypropylene	105	0·5

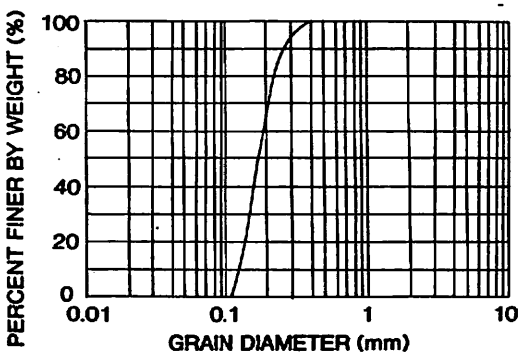

Fig. 6. Grain-size distribution curve of Toyoura sand.

uniform sand mainly composed of quartz with subangular to angular grains. The mean diameter is 0·16 mm, the specific gravity is 2·64, and the uniformity coefficient is 1·46. The grain-size distribution of Toyoura sand is shown in Fig. 6.

4 PREPARATION OF GEOTEXTILE AND SOIL SPECIMENS

An aspect ratio of 8 has been used for most of the tests in order to maintain as closely as possible a plane-strain condition. Each geotextile specimen was reinforced with an epoxy at the two ends (see Fig. 7). A slow-hardening epoxy (Araldite® AW106 with hardener HV953U) was used to reinforce the thicker geotextiles (i.e. the needle-punched and spun-bonded geotextile) in order to give it ample time to penetrate into the fiber matrix before setting, while a rapid-hardening epoxy was used for the thinner geotextile (i.e. the heat-bonded geotextile). A clearly defined unreinforced zone of the geotextile specimen was made possible by adhering a strip of Scotch tape along the edge of the unreinforced zone before applying the epoxy.

After the epoxy had set, circular holes with a diameter of 1 cm were drilled at regular intervals of 4·5 cm in the two reinforced zones of the

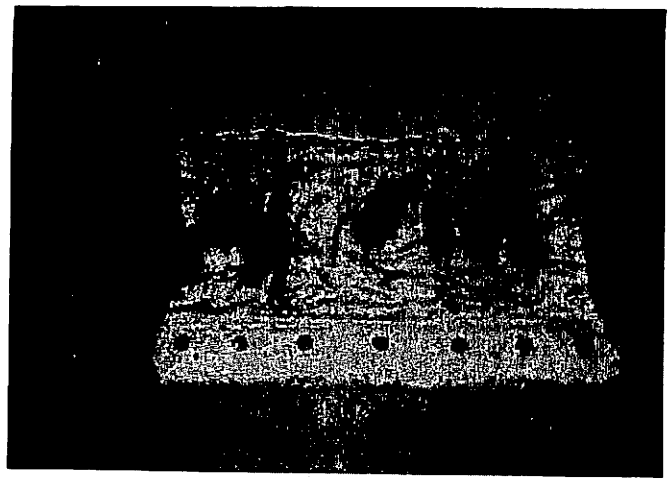

(a)

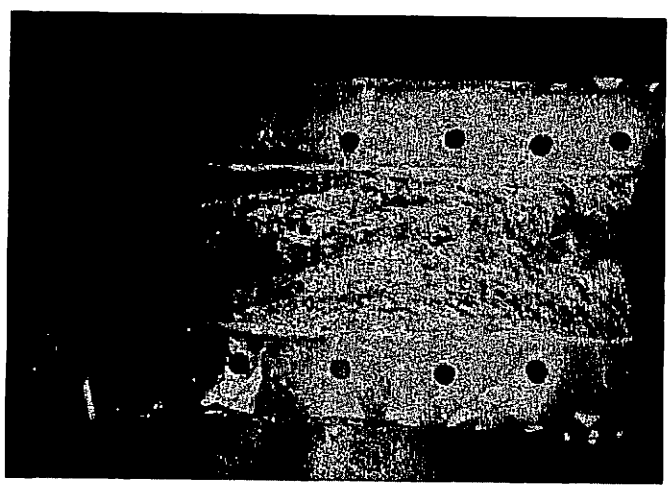

(b)

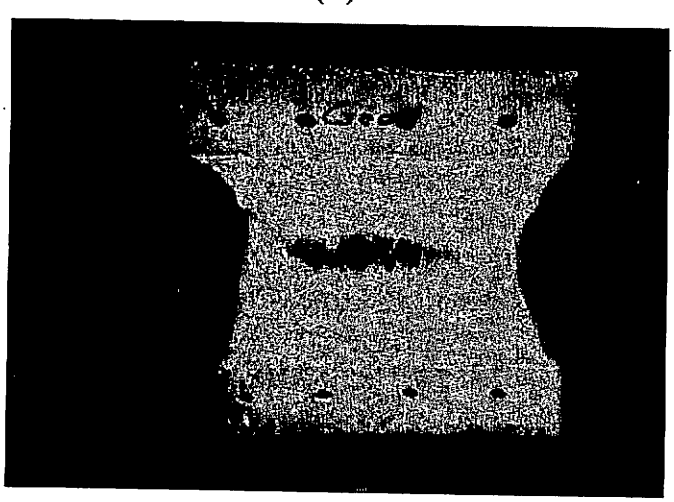

(c)

Fig. 7. Geotextile specimens after test. (a) Spun-bonded, $W/L = 8$ (30 cm/3·75 cm); (b) heat-bonded, $W/L = 8$ (30 cm/3·75 cm); (c) needle-punched, $W/L = 2$ (20 cm/10 cm).

geotextile specimens. Through the drilled holes, the geotextile specimen was secured between clamp jaws using nut, bolt and washer. A total of 14 screws, seven on each jaw, were used to give a uniform tensile load distribution across the width of the geotextile (see Fig. 4b). Due to the high rigidity of the hardened epoxy relative to the unreinforced geotextile, the clamping system functioned effectively, as evidenced by the drilled holes remaining intact after each test.

In the in-soil tests, the geotextile, after having been affixed to the clamps, was confined on both sides using two frozen cakes of Toyoura sand and was then enclosed in a rubber membrane. The frozen cakes were prepared beforehand at a void ratio of 0·66 by pluviating air-dried sand particles through air into a cubical mold with inner dimensions equal to those of the cake. The surface area of the cake was 30 cm × 3·75 cm and 20 cm × 10 cm, respectively, which was equal to that of the geotextile specimen at an aspect ratio of 8 and 2. Water was then introduced from the bottom of the mold to moisten the sand and subsequently dewatered before refrigeration. In this study, cubical-shaped soil cakes were used to ensure that the stress acting on the geotextile was sufficiently uniform when confined and stressed. In addition, a small thickness (0·8 cm) of the cake was selected so that the tensile resistance due to the confining soil would be minimized. The test specimen was then confined by a partial vacuum and left overnight for the frozen sand to thaw and to become air-dried again before starting the test.

5 TESTING PROGRAM

Three series of tests, each with a different method of confinement, were performed on these three types of non-woven geotextile. Table 2 gives a summary of the testing program.

For the in-air tests on the spun-bonded geotextile, specimens with aspect ratios of 5, 6, 8 and 12 (at a width of 30 cm) were used. These tests were conducted to ensure that a sufficiently large aspect ratio was used for the confined tests of this geotextile.

Figure 8 shows the load–deformation relationship of the spun-bonded non-woven geotextile at different aspect ratios. The axial strain is defined as the ratio of the elongation to the original gage length of the geotextile specimen. It is seen from these curves that slightly greater stiffness was obtained with a larger aspect ratio. However, the results for the aspect ratios of 8 and 12 were considered sufficiently close, and an aspect ratio of 8 was selected for the tests confined with membrane and soil.

Table 2
Testing Program

Group	*Geotextile type*	*Aspect ratio*	*Confining pressure (kgf/cm²)*
In-air test	Spun-bonded	5, 6, 8, 12	0
	Needle-punched	2, 8 (2 tests)	0
	Heat-bonded	8	0
In-soil test	Spun-bonded	8	0·80
	Needle-punched	2 (2 tests)	0·56
		8	0·75
	Heat-bonded	8	0·75
In-membrane test	Spun-bonded	8	0·50
		8 (2 tests)	0·80
	Needle-punched	2	0·56, 0·75
		8	0·75
	Heat-bonded	8	0·75

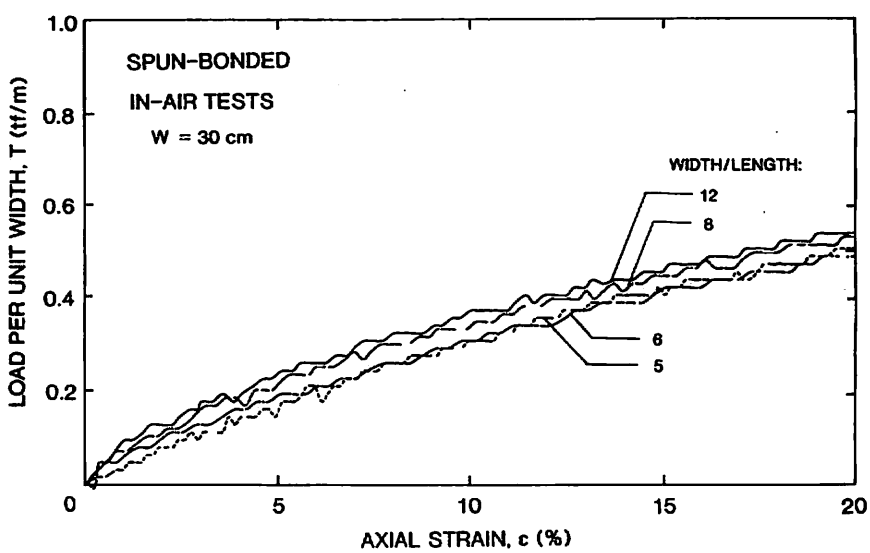

Fig. 8. In-air test results for spun-bonded geotextiles at different aspect ratios.

For the in-soil test of the spun-bonded geotextile, a confining pressure of 0·8 kgf/cm² (78·48 kN/m²) was used. For the in-membrane test, in addition to the confining pressure of 0·8 kgf/cm², a confining pressure of 0·5 kgf/cm² (49·05 kN/m²) was also used to examine the effect of confinement by different pressures. Two in-membrane tests were performed at 0·8 kgf/cm² to check the test repeatability.

In the tests performed for the needle-punched geotextile, aspect ratios of 2 (20 cm/10 cm) and 8 (30 cm/3·75 cm) were used for the in-air,

in-membrane and in-soil tests. The aspect ratio of 2 was also selected because it is a dimension suggested by many researchers and has been widely used in practice. Confining pressures of 0·56 kgf/cm^2 (54·94 kN/m^2) and 0·75 kgf/cm^2 (73·58 kN/m^2) were used for the tests with an aspect ratio of 2, and 0·75 kgf/cm^2 for the tests with an aspect ratio of 8.

For the heat-bonded geotextile, an in-air, in-membrane and in-soil test was performed only for an aspect ratio of 8 (30 cm/3·75 cm). In the confined tests, a pressure of 0·75 kgf/cm^2 was used.

Triaxial extension tests were performed on Toyoura sand alone enclosed by a rubber membrane but under otherwise identical conditions to those used in the in-soil tests. In addition, a test with only the membrane was performed to evaluate its tensile resistance. These tests enabled the load–deformation relationships of the in-soil and in-membrane tests to be corrected for the exact loads applied to the geotextile.

For all the tests, the geotextiles were strained in their machine direction at a constant strain rate of 2% per min until failure occurred. The room temperature was maintained at around 20°C for all the tests.

6 EFFECT OF SOIL TENSILE RESISTANCE ON IN-SOIL TEST RESULTS

Figures 9a and 9b show the load–deformation relationship of the in-soil test performed on the spun-bonded geotextile at small and large strain levels, respectively. Also shown are the resistances offered by the soil and the rubber membrane. It can be seen in Fig. 9a that at small strain levels, the tensile resistance of the soil accounted for a relatively large portion of the measured load, about 20% of the applied load at 5% strain level. Therefore, the measured loads, without taking into account the soil resistance, could significantly overestimate the stiffness of geotextiles at small strains, especially if the geotextile is weak. However, its effect on the failure load was not as significant, as the soil resistance was only about 8% of the measured load at failure. Therefore, it was considered that despite the uncertainty about the triaxial extension strength of sand as mentioned previously, the strength of the geotextile in the in-soil test could be evaluated with sufficient accuracy using this apparatus. The resistance taken by the rubber membrane, on the other hand, was negligibly small when compared to the measured loads in the in-membrane test.

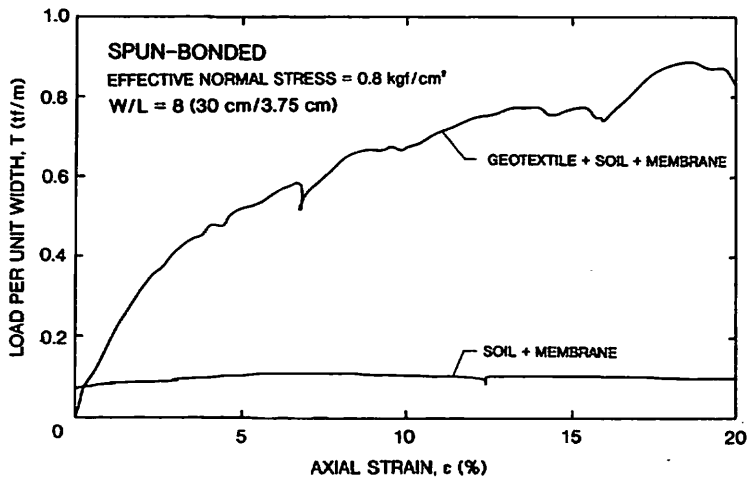

(a)

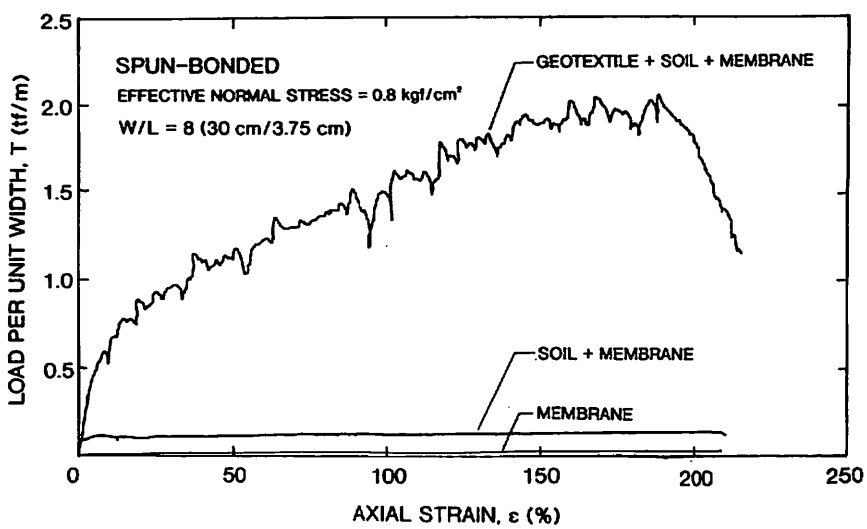

(b)

Fig. 9. In-soil test results for (a) a spun-bonded geotextile up to 20% strain (b) a spun-bonded geotextile up to failure.

7 EFFECT OF DIFFERENT MATERIALS ON STRESS CONFINEMENT

The load–deformation relationships of the spun-bonded, the needle-punched, and the heat-bonded geotextiles obtained from the in-soil tests are shown in Figs 10–13. The loads shown in the figures have been corrected by subtracting the resistance of the soil and membrane from the applied tensile loads. The geotextile specimens used in the tests were

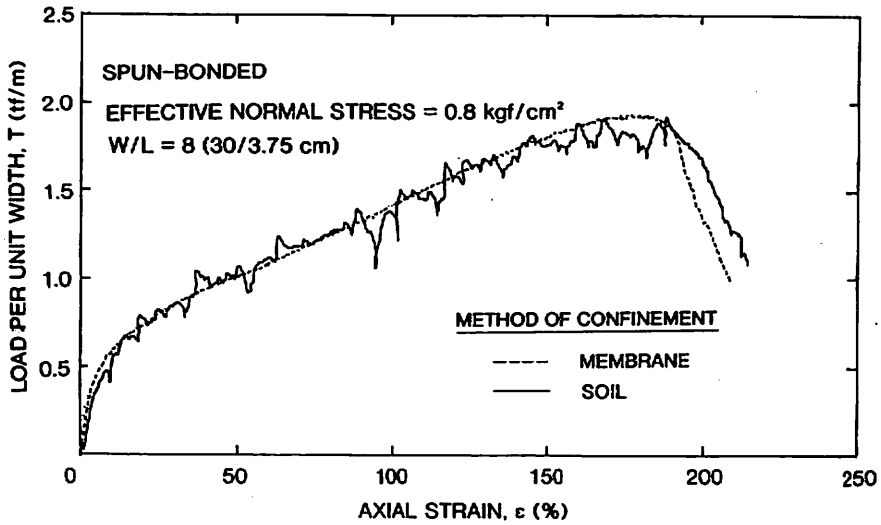

(a)

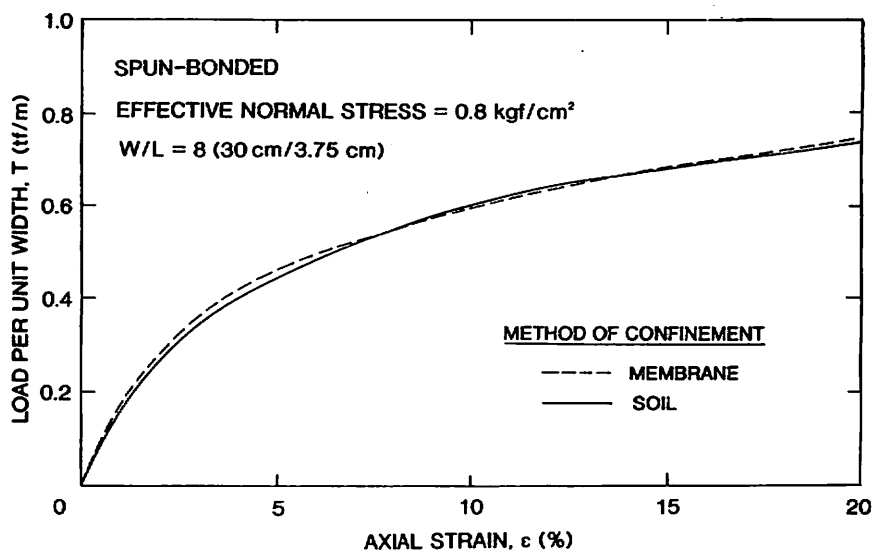

(b)

Fig. 10. In-membrane and in-soil test results for (a) a spun-bonded geotextile (W/L = 8, 250% strain level), (b) a spun-bonded geotextile (W/L = 8, 20% strain level).

of an aspect ratio of 8 except that of Fig. 12 which was 2. A slight fluctuation was observed in the test results (Fig. 10a). This may be due to a lack of uniform stress confinement on the geotextile when the soil was largely strained and distorted. That is, if the normal pressure acting on some part of the geotextile is smaller than the average, this portion of the geotextile would deform largely or would even exhibit a smaller stiffness and strength than in the case of uniform pressure distribution.

Also shown in Figs 10–13 are the load–deformation relationships of

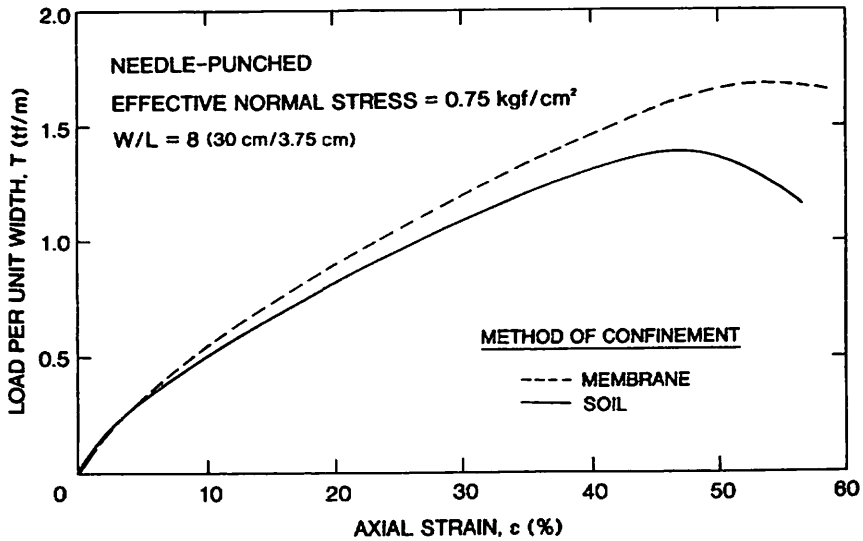

Fig. 11. In-membrane and in-soil test results for a needle-punched geotextile (W/L = 8, 60% strain level).

the geotextiles obtained from the in-membrane tests. No significant difference exists between the in-membrane and the in-soil tests was seen for the results at both small and large strain levels. For the needle-punched geotextile, it is seen that as the strains are larger than about 5%, the geotextile exhibited a greater stiffness in the in-membrane tests than in the in-soil test.

As shown in Fig. 14, very close agreement was obtained for the results of the two in-membrane tests performed on the spun-bonded geotextile confined at a pressure of 0·8 kgf/cm^2. This indicates that the in-membrane test is very repeatable.

8 EFFECTS OF STRESS CONFINEMENT ON LOAD-DEFORMATION RELATIONSHIPS

In this section, only the load-deformation relationship of the geotextiles obtained from the in-membrane tests is discussed. Figures 15–17 show the load-deformation relationships of the three geotextiles at different confining pressures. It is seen in Figs 15 and 16 that the confinement gave a greater stiffness and strength for the spun-bonded and needle-punched geotextiles. Their failure strains were not much affected by the confining pressure. However, as may be seen in Fig. 17, the confinement has little effect on the heat-bonded geotextiles.

The spun-bonded and needle-punched geotextiles have a relatively open structure. When subjected to a confining pressure, the structure will

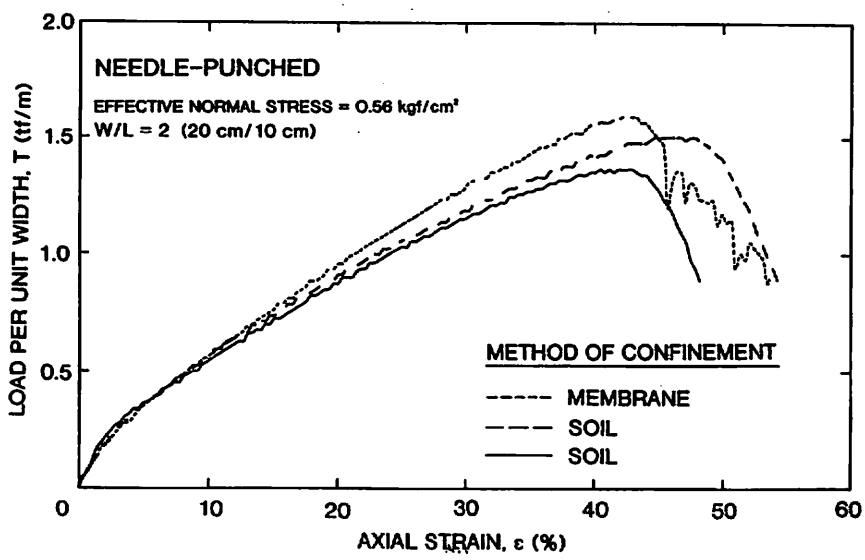

(a)

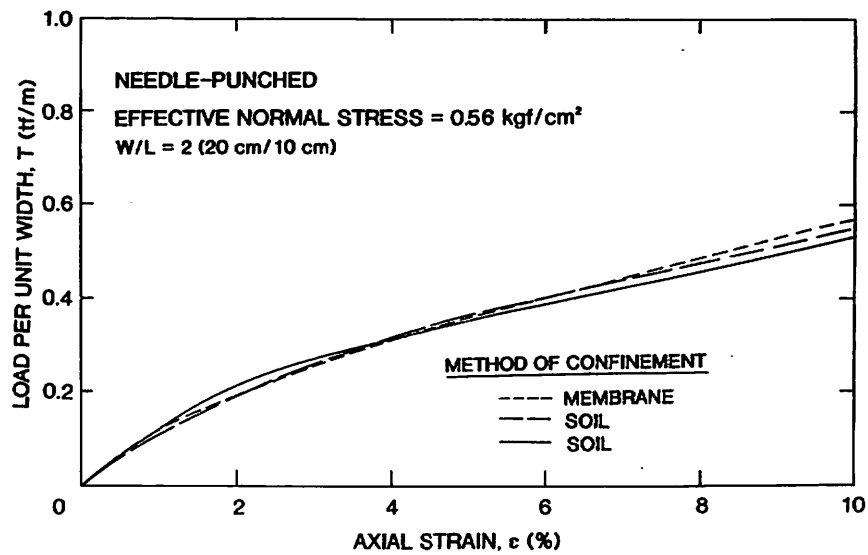

(b)

Fig. 12. In-membrane and in-soil test results for (a) a needle-punched geotextile (W/L = 2, 60% strain level), (b) a needle-punched geotextile (W/L = 2, 10% strain level).

assume a more compact state and give rise to a higher stiffness and strength compared with the unconfined condition. The heat-bonded geotextile, on the other hand, has a compact structure due to the manufacturing process. Consequently, the load-deformation relationship for the unconfined test is similar to that of the confined test.

Since the geotextiles used in this study were different from those reported in the literature, a direct comparison with other test results

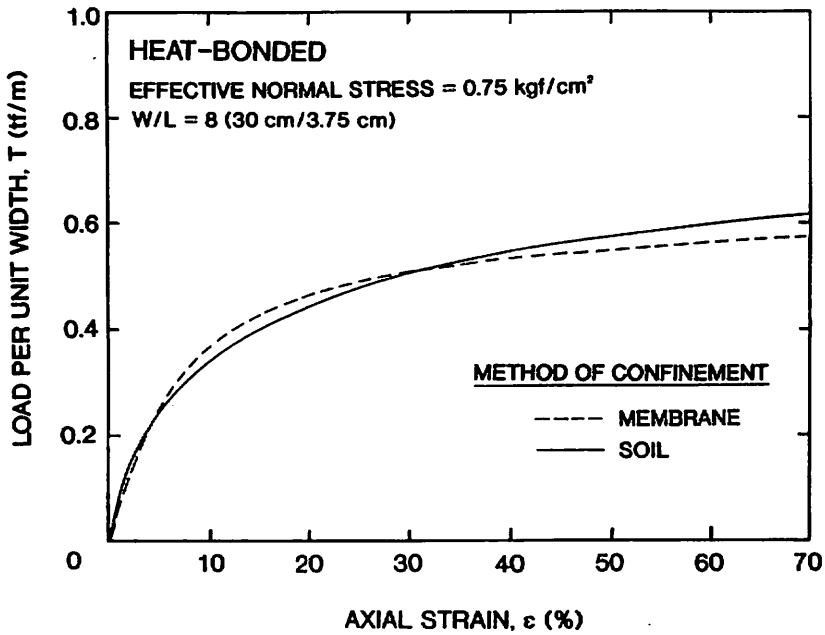

Fig. 13. In-membrane and in-soil test results for a heat-bonded geotextile (W/L = 8, 70% strain level).

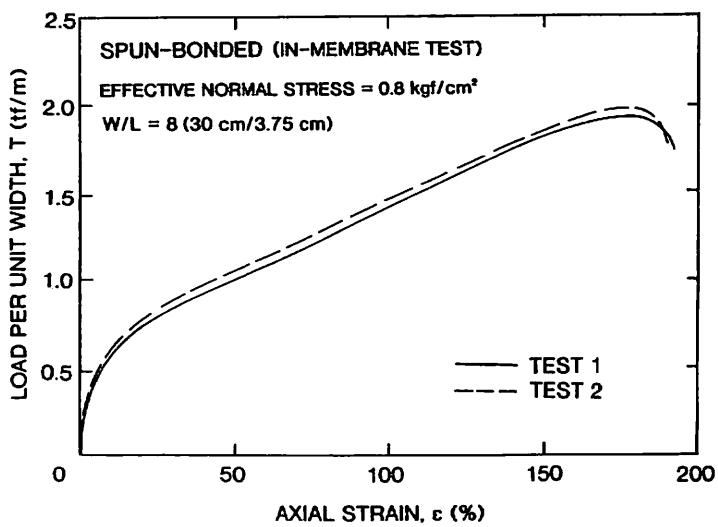

Fig. 14. Repeatability of in-membrane test.

cannot be made. It should be noted, however, that McGown *et al.* (1981, 1982) and Nishigata & Yamaoka (1989) reported a significant increase in the stiffness and strength and a reduction in failure strain due to soil confinement for heat-bonded geotextiles. It is believed that their results yielded an overestimation of the tensile resistance of the geotextiles.

For the spun-bonded and needle-punched geotextiles tested at an aspect ratio of 8, the unconfined and confined tests gave a similar mode

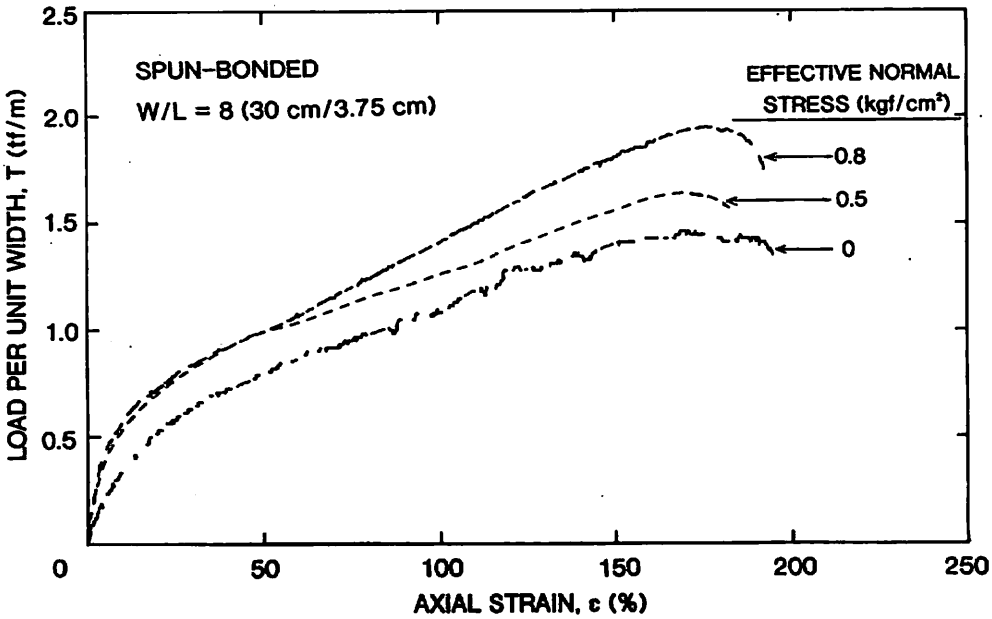

Fig. 15. Load-deformation relationship of a spun-bonded geotextile ($W/L = 8$).

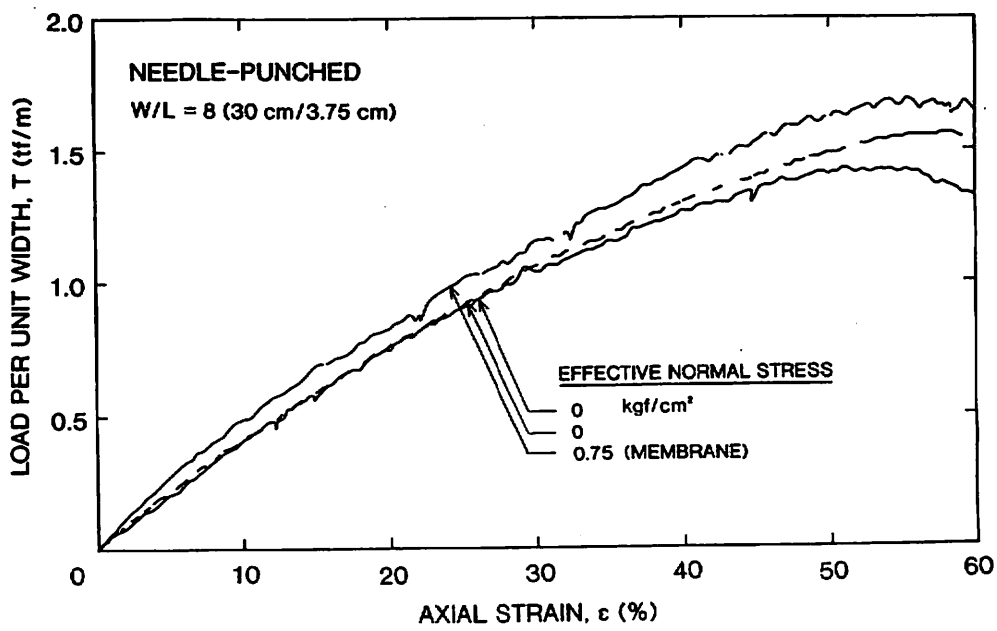

Fig. 16. Load-deformation relationship of a needle-punched geotextile ($W/L = 8$).

of failure. A rupture line was observed to initiate at the side edges of the specimens which then propagated horizontally toward the center (see Fig. 7(a) and (b)). However, for the needle-punched geotextile tested at an aspect ratio of 2, the rupture line was observed to initiate near the center of the specimens (see Fig. 7(c)). This could be because large

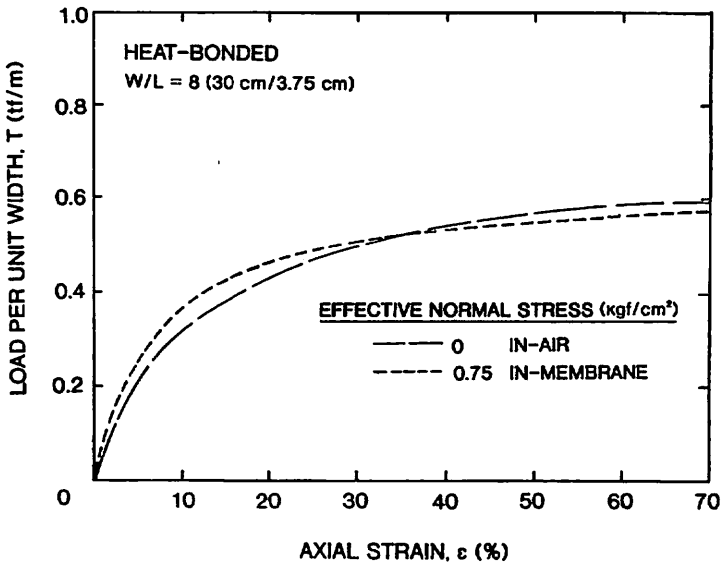

Fig. 17. Load-deformation relationship of a heat-bonded geotextile ($W/L = 8$).

amount of compressive lateral straining (necking) occurred at the two sides, accompanied by large axial straining, at the aspect ratio of 2. For the specimens with the aspect ratio of 8, a near plane-strain condition inhibited the lateral straining at the two sides, as shown in Fig. 18.

Figure 19 shows the load-deformation relationships of the needle-punched geotextile tested under different confining pressures, with specimens of an aspect ratio of 2 (at a width of 20 cm). When compared with Fig. 16 for the same geotextile at an aspect ratio of 8, it is found that the stress-confinement effect was more significant for the specimens at an aspect ratio of 2. Under unconfined conditions, the stiffness and strength of the needle-punched geotextile at an aspect ratio of 8 were

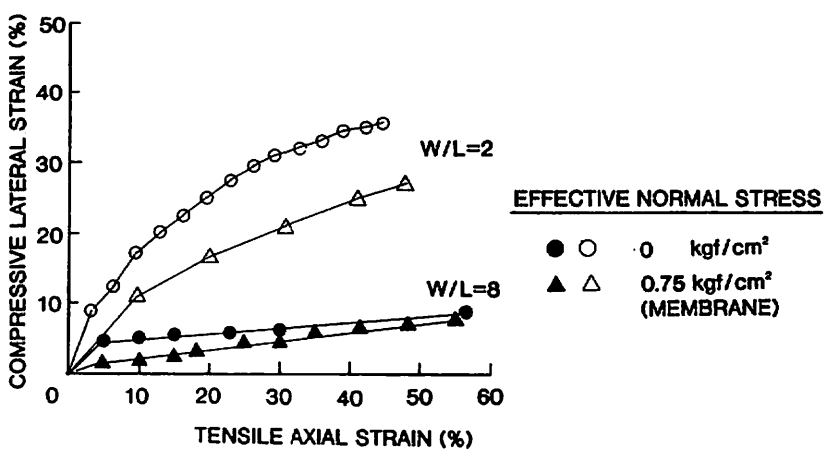

Fig. 18. Lateral straining of a needle-punched geotextile.

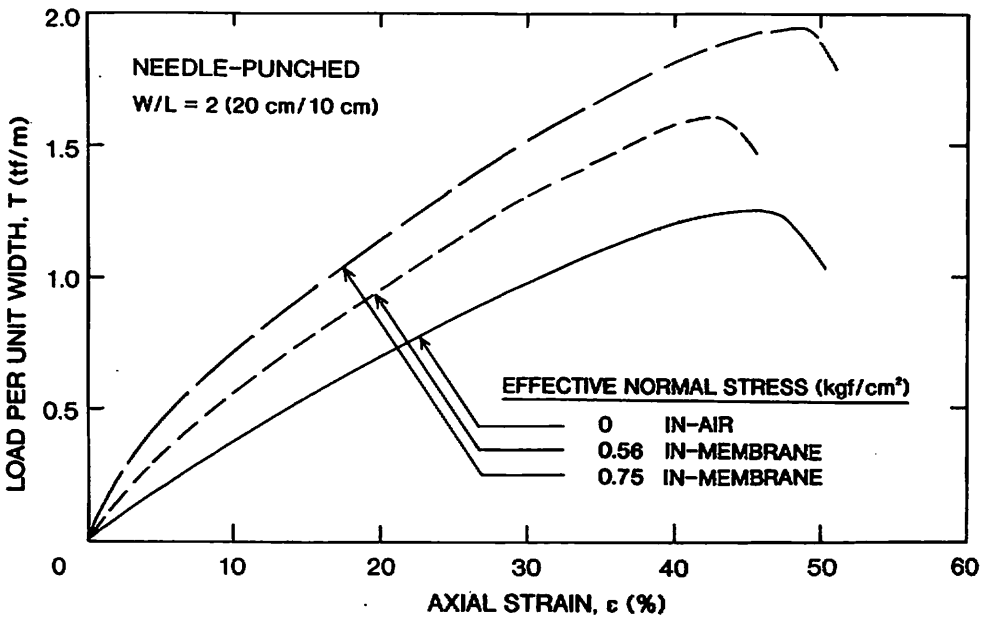

Fig. 19. Load-deformation relationship of a needle-punched geotextile (W/L = 2).

rather close to those of 2, but under confined conditions, they were less than those at 2. The failure strain for the geotextile at an aspect ratio of 8 was greater than that at 2. Note also that different widths (20 cm and 30 cm) of the specimens were used for the two aspect ratios. The discrepancies in the results may be attributed at least to the following:

(1) the difference in the failure mode (failure initiated at the edges or at the center), and
(2) the difference in stress-confinement effect as a result of lateral straining.

These two factors may, however, be related to the difference in length and/or the width of the specimens.

9 MATHEMATICAL MODELS OF LOAD-DEFORMATION RELATIONSHIP OF GEOTEXTILE

Numerical methods, especially the finite element method, have gained popularity in the analysis and design of geotextile-reinforced soil structures. Most of the analyses to date have been performed by assuming the geotextile to be linear elastic, but the finite element method offers great flexibility to accommodate non-linear and stress-dependent geotextile stress-strain relationships. Several mathematical equations have been used to express the load-deformation relationship of

geotextiles, among which hyperbolic and polynomial functions are most widely used.

9.1 Hyperbolic model

The load–deformation relationship can be expressed by a hyperbolic model as:

$$T = \frac{\varepsilon}{a + b\varepsilon} \tag{1}$$

where T is the load per unit width, ε is the axial strain in tension, and a and b are the parameters to be determined from the experimental results. By transforming the results in the form of a ε/T versus ε relationship, as suggested by Konder (1963) for simulating the soil stress–strain relationship, the parameters a and b are obtained as the intercept at the ordinate and the slope of the graph, respectively, whose reciprocals are the initial tensile modulus, E_i, and the failure load (ultimate load), T_f, of the geotextile. Instead of the graphical method, the least-squares method can also be conveniently employed. The initial modulus and the failure load may be dependent on the effective normal stress (confining pressure), σ_n', which may be represented using an exponential equation or a linear equation as follows:

$$1/a = E_i = y(1{\cdot}0 + \sigma_n')z \tag{2}$$

$$1/b = T_f = y'(1{\cdot}0 + \sigma_n')z' \tag{3}$$

or

$$1/a = E_i = y + z\sigma_n' \tag{4}$$

$$1/b = T_f = y' + z'\sigma_n' \tag{5}$$

where y, z, y' and z' are the constants to be obtained from a series of load–extension tests. The equations are formulated in such a way that the values of y and y' can be directly determined from the results of in-air tests. Substitution of these equations into eqn (1) gives a non-linear stress-dependency equation for the load–deformation relationship of geotextiles. Li *et al.* (1990) have used this hyperbolic model with parameters expressed by eqns (2) and (3) in the analysis of a reinforced embankment.

9.2 Polynomial model

In the polynomial model, the load–deformation relationship is expressed as

$$T = a_1\varepsilon + a_2\varepsilon^2 + \ldots + a_n\varepsilon^n \quad (6)$$

where a_i are the polynomial constants and n is the order of the polynomial. The polynomial constants may be determined using the least-squares method. Second- and third-order polynomials have been used by some researchers (for example, by Andrawes *et al.*, 1980, 1982; Gray *et al.*, 1989).

The polynomial constants may also be related to the load–deformation parameters of a geotextile, such as the initial modulus, E_i, failure load, T_f, and failure strain, ε_f, by satisfying some boundary conditions, as given in Table 3. These boundary conditions are: the tangent modulus equals the initial modulus at zero strain, the tangent modulus is zero and the load is the failure load at the failure strain. Chalaturnyk *et al.* (1990) used the second-order polynomial, expressed by the parameters E_i and ε_f, which was named by them as the non-linear quadratic model in the analysis of reinforced soil slope. However, it was found in this study that when the parameters which satisfy these boundary conditions are used to represent the load–deformation relationship, the results deviate considerably at intermediate strain levels for some geotextiles. Therefore, for the descriptions in the subsequent sections, the polynomial constants were obtained from the least-squares method so that a better fit of the overall relationship can be obtained.

10 MATHEMATICAL REPRESENTATION OF TEST RESULTS

Figures 20–22 show the results of the load–deformation relationships of the three geotextiles fitted by the hyperbolic and polynomial models using the least-squares method. The constants for the models fitted by the least-squares method are given in Table 4, in which the loads are expressed in tonnes-force per meter (1 tf/m = 9·81 kN/m) and strain in percentage. It has to be noted that these constants give a better fit of the overall load–deformation relationship when compared to those which

Table 3
Relationship between Polynomial Constants and Load–Deformation Parameters

Order of polynomial	*Mathematical equation*	a_1	a_2	a_3
2nd	$T = a_1\varepsilon + a_2\varepsilon^2$	E_i	$-1/(2\varepsilon_f)\,E_i$	—
3rd	$T = a_1\varepsilon + a_2\varepsilon^2 + a_3\varepsilon^3$	E_i	$1/(\varepsilon_f^2)\,(3T_f - 2E_i\varepsilon_f)$	$1/(\varepsilon_f^3)\,(E_i\varepsilon_f - 2T_f)$

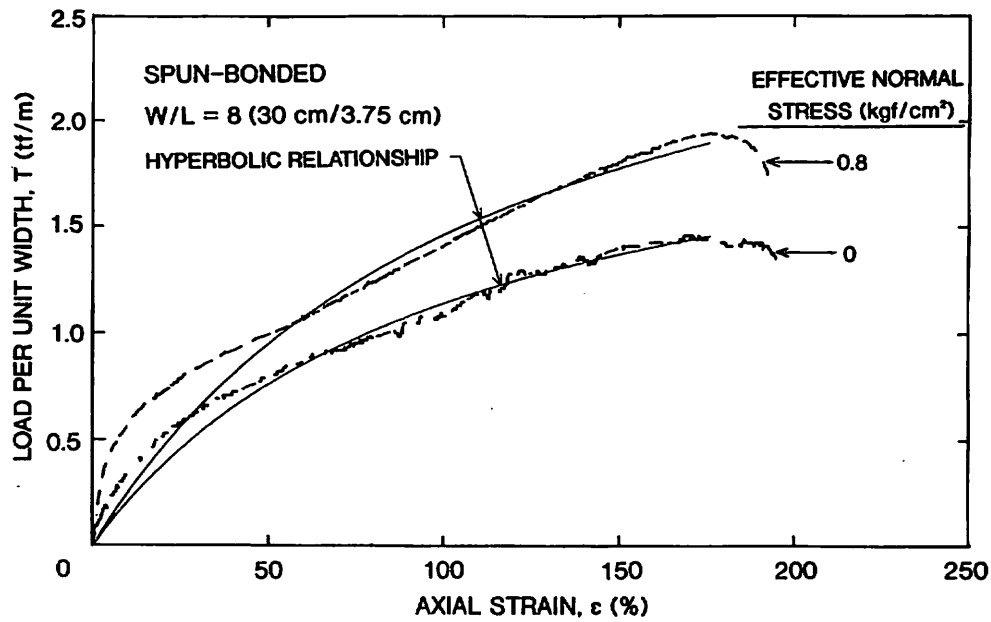

(a)

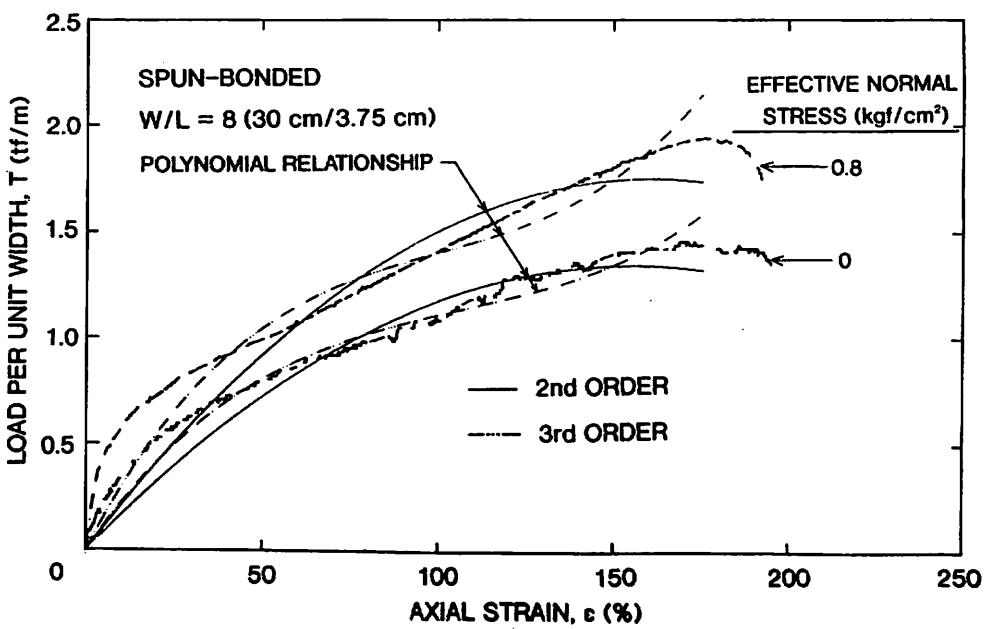

(b)

Fig. 20. Load-deformation relationship of (a) a spun-bonded geotextile represented using hyperbolic models ($W/L = 8$), (b) a spun-bonded geotextile represented using polynomial models ($W/L = 8$).

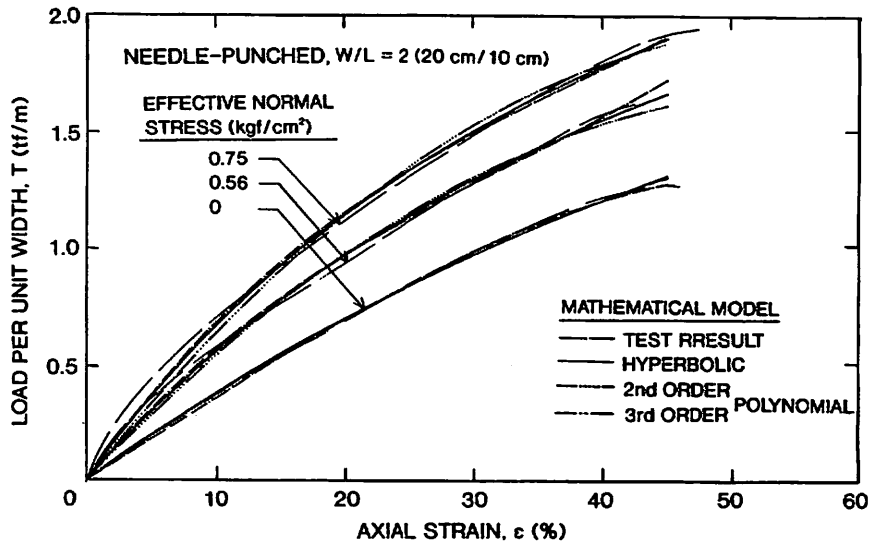

Fig. 21. Load-deformation relationship of a needle-punched geotextile represented using different mathematical models (W/L = 2).

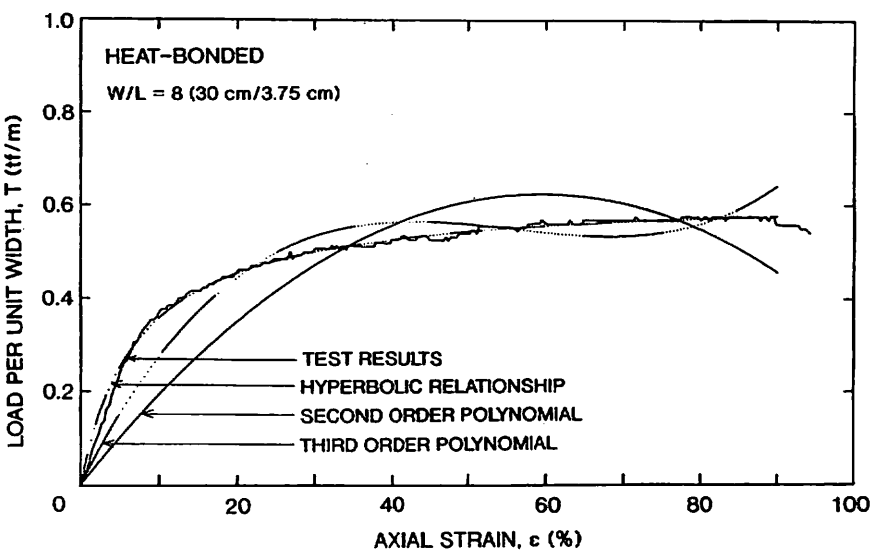

Fig. 22. Load-deformation relationship of a heat-bonded geotextile represented using different mathematical models (W/L = 8).

satisfy only certain boundary conditions. By comparing these constants to that of the geotextile parameters in Table 3, it can be seen that they do not strictly correspond to each other.

From these figures, it is seen that the accuracy of these mathematical models for representing the load-deformation relationship differs from

Table 4
Constants for Hyperbolic and Polynomial Models

Geotextile	*Confining pressure (kgf/cm²)*	*Constants*		
(i) *Hyperbolic model*		a	b	
Spun-bonded	0	43·346	0·439	
	0·50	31·493	0·438	
	0·80	36·122	0·319	
Needle-punched	0	24·295	0·225	
	0·56	15·642	0·254	
	0·75	12·627	0·245	
Heat-bonded	0·75	11·938	1·600	
(ii) *Second-order polynomial model*		a_1	a_2	
Spun-bonded	0	$1·8 \times 10^{-2}$	$-5·7 \times 10^{-5}$	
	0·50	$2·2 \times 10^{-2}$	$-8·2 \times 10^{-5}$	
	0·80	$2·2 \times 10^{-2}$	$-6·9 \times 10^{-5}$	
Needle-punched	0	$3·9 \times 10^{-2}$	$-2·3 \times 10^{-4}$	
	0·56	$5·9 \times 10^{-2}$	$-5·1 \times 10^{-4}$	
	0·75	$6·9 \times 10^{-2}$	$-6·1 \times 10^{-4}$	
Heat-bonded	0·75	$2·1 \times 10^{-2}$	$-1·8 \times 10^{-4}$	
(iii) *Third-order polynomial model*		a_1	a_2	a_3
Spun-bonded	0	$2·5 \times 10^{-2}$	$-1·9 \times 10^{-4}$	$6·0 \times 10^{-7}$
	0·50	$3·4 \times 10^{-2}$	$-3·2 \times 10^{-4}$	$10·5 \times 10^{-7}$
	0·80	$3·3 \times 10^{-2}$	$-2·8 \times 10^{-4}$	$9·3 \times 10^{-7}$
Needle-punched	0	$3·6 \times 10^{-2}$	$3·7 \times 10^{-5}$	$-4·4 \times 10^{-6}$
	0·56	$6·7 \times 10^{-2}$	$-1·2 \times 10^{-3}$	$1·2 \times 10^{-5}$
	0·75	$8·0 \times 10^{-2}$	$-1·4 \times 10^{-3}$	$1·2 \times 10^{-5}$
Heat-bonded	0·75	$3·3 \times 10^{-2}$	$-6·4 \times 10^{-4}$	$3·8 \times 10^{-6}$

Load per unit width in tf/m; strain as percentage.

one geotextile to another. For the spun-bonded geotextile, neither the hyperbolic nor the polynomial model accurately fitted the entire range of experimental results. On the other hand, both models simulated considerably better the load–deformation relationships of the needle-punched geotextile, of which the strain ranges up to failure were much smaller than those of the spun-bonded geotextile. For the heat-bonded geotextile, the hyperbolic model fitted the experimental data better than the polynomial model.

In performing stress analysis of reinforced soil structures under design loads, the stiffness at small strain levels is generally more important. A better representation of the load-deformation relationship can be obtained by fitting a mathematical model over the range of strain of interest. In this case, the parameter b in the hyperbolic model will no longer be the reciprocal of the ultimate load. For example, the strains up to 20% for the spun-bonded geotextile fitted by the hyperbolas and the polynomials are shown in Figs 23a and 23b, respectively and the related constants are given in Table 5. The hyperbolic and the third-order polynomial models fitted the load-deformation relationship in this selected range of strain relatively well. But, the hyperbolic model is considered to be simulating the load-deformation relationship better than the third-order polynomial model. Moreover, the stress-confinement effect of the geotextile, as discussed later in Section 11, can be conveniently expressed by eqns (2)–(5) and incorporated into the hyperbolic model.

11 RELATIONSHIP BETWEEN LOAD-DEFORMATION PARAMETERS AND CONFINING PRESSURE

Figures 24 and 25 show the relationship between the secant tensile modulus, E_{sec}, and the axial strain, ε, for the spun-bonded ($W/L = 8$) and needle-punched ($W/L = 2$) geotextiles at different confining pressures. It is evident that the secant modulus, E_{sec}, increased substantially under the application of confining pressure, especially at small strain levels.

Figures 26 and 27 show the relationships between the initial tensile modulus (tf/m) and confining pressure (kgf/cm^2), and the failure load (tf/m) and confining pressure (kgf/cm^2) for the spun-bonded and needle-punched geotextiles, respectively. A linear relationship appears to be sufficient in representing the stress-dependency behavior of the initial modulus and the failure load at the examined stress levels. That is, for the spun-bonded geotextile,

$$E_i = 19{\cdot}872\,\sigma_n' + 9{\cdot}313 \tag{7}$$

$$T_f = 0{\cdot}566\,\sigma_n' + 1{\cdot}435 \tag{8}$$

and for the needle-punched geotextile,

$$E_i = 15{\cdot}561\,\sigma_n' + 7{\cdot}372 \tag{9}$$

$$T_f = 0{\cdot}855\,\sigma_n' + 1{\cdot}228 \tag{10}$$

Comparing the measured tensile moduli of the geotextiles with those

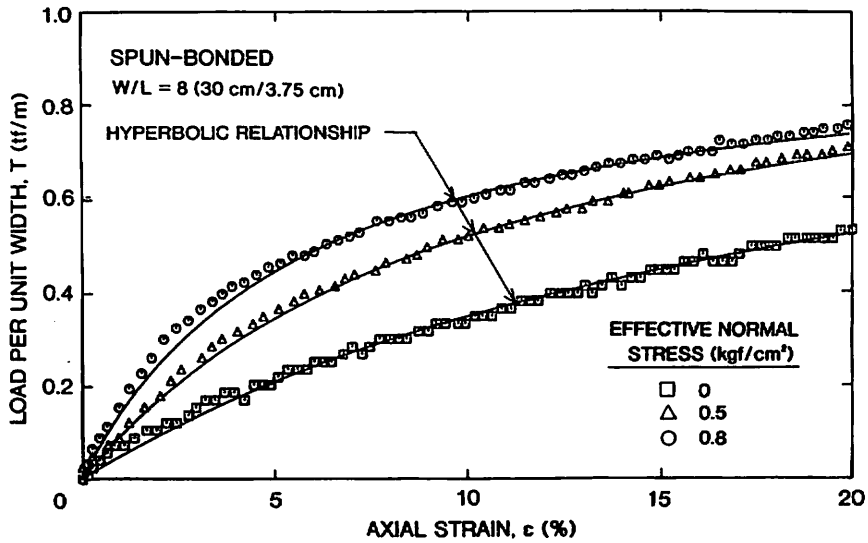

(a)

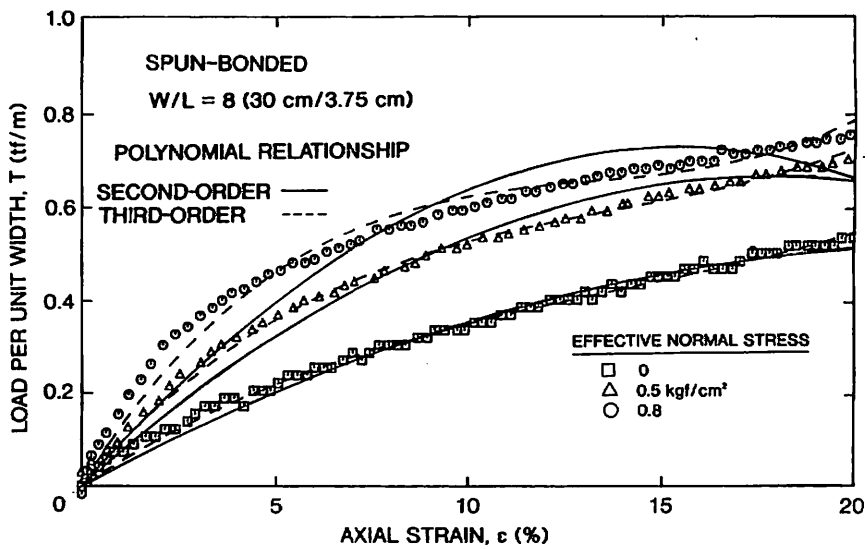

(b)

Fig. 23. Load-deformation relationship of (a) a spun-bonded geotextile represented using hyperbolic models at small strain ($W/L = 8$), (b) a spun-bonded geotextile represented using polynomial models at small strain ($W/L = 8$).

fitted by the hyperbolic and polynomial models (see Figs 24, 25, 26a and 27a, it may be seen that while these model parameters simulated the overall behavior fairly well (see Figs 21–23), they underestimated the values of initial moduli of the geotextiles.

The failure loads, on the other hand, were overestimated by the hyperbolic model (Figs 26b and 27b). A reduction factor of 0·6 and 0·4,

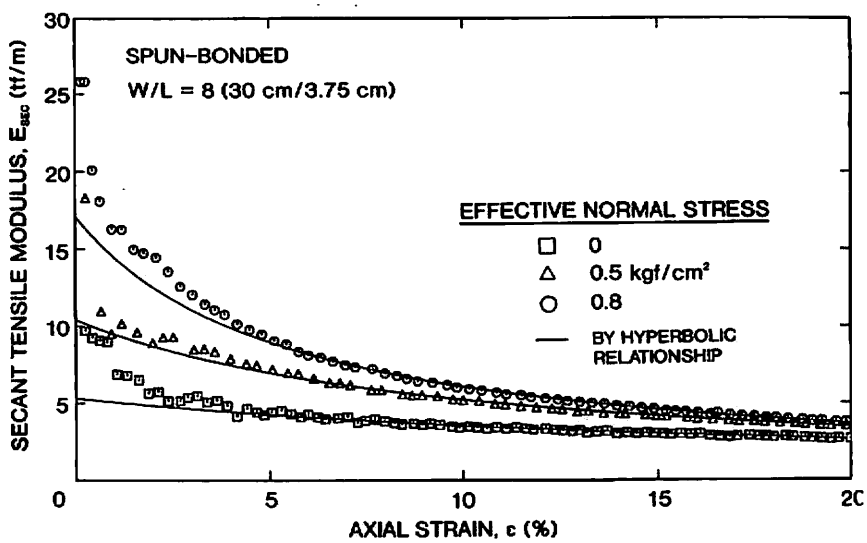

Fig. 24. Relationship between secant tensile modulus and strain for a spun-bonded geotextile ($W/L = 8$).

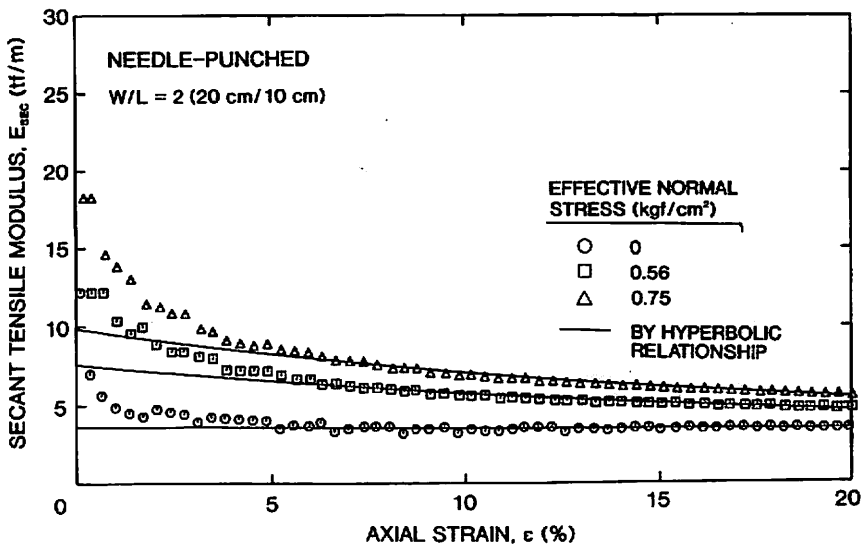

Fig. 25. Relationship between secant tensile modulus and strain for a needle-punched geotextile ($W/L = 2$).

for the spun-bonded and needle-punched geotextiles, respectively, needs to be introduced to bring the failure loads to those of the experimental results.

These results showed that the parameters E_i and T_f used in these models, which were determined from the hyperbolic relationship, are not the actual material properties. Similar results were obtained for the parameters determined from the polynomial relationships. Other

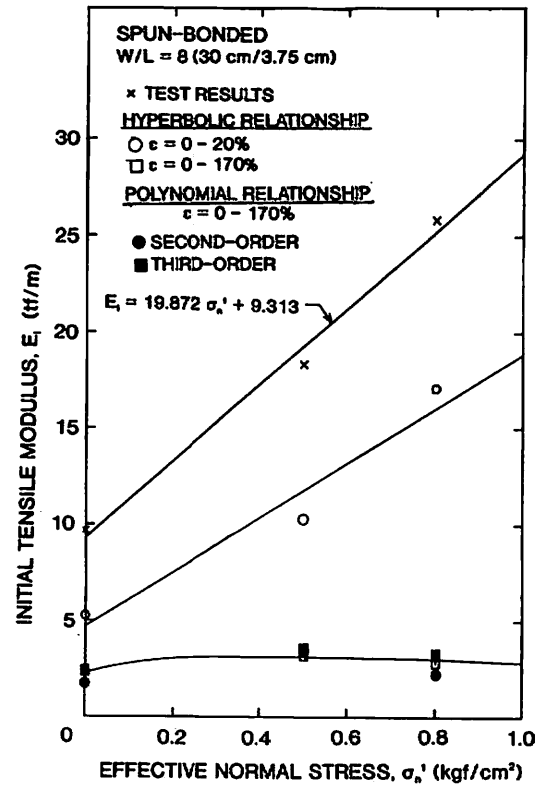

(a)

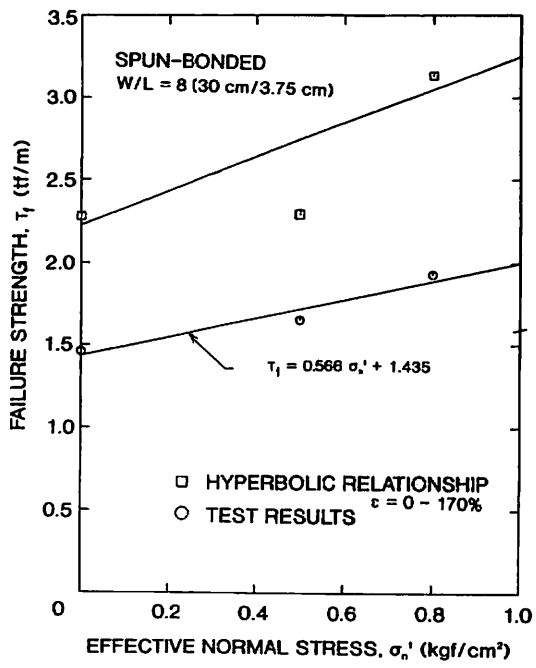

(b)

Fig. 26. Relationship between (a) initial tensile modulus and confining pressure for a spun-bonded geotextile (W/L = 8), (b) failure load and confining pressure for a spun-bonded geotextile (W/L = 8).

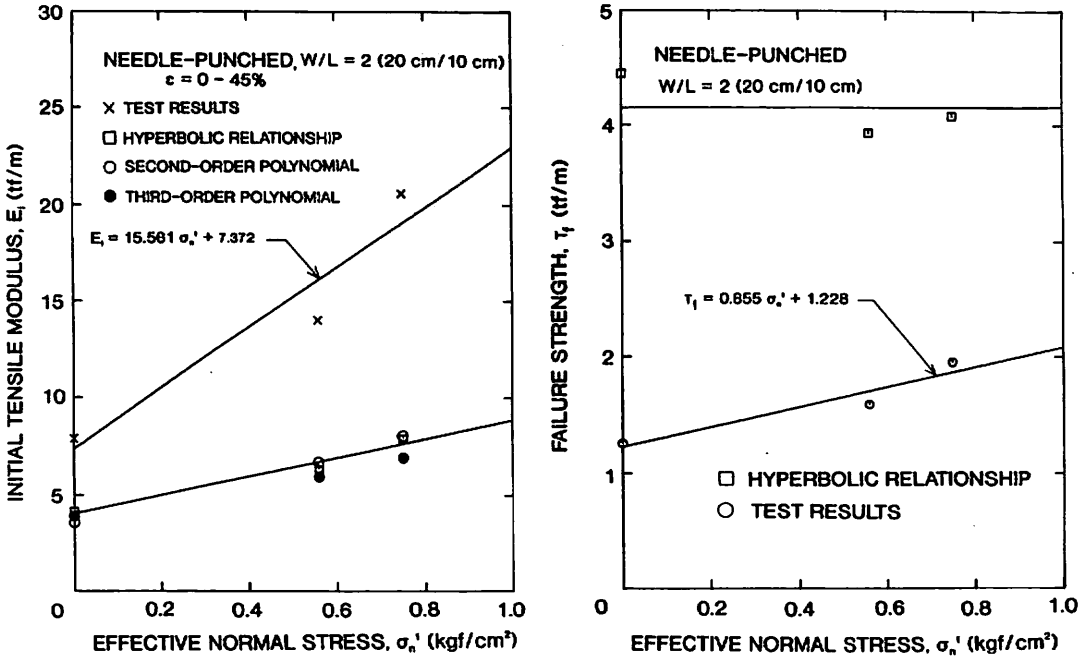

Fig. 27. Relationship between (a) initial tensile modulus and confining pressure for a needle-punched geotextile (W/L = 2), (b) failure load and confining pressure for a needle-punched geotextile (W/L = 2).

mathematical functions need to be formulated for a better simulation of the overall load-deformation relationships.

12 CONCLUSIONS

From the results of this study, it is concluded that:

(1) The test apparatus developed in this study is capable of measuring the load-deformation properties of geotextiles consistently under in-air, in-membrane and in-soil conditions.

(2) In the confined tests, using a membrane for stress confinement of the geotextile specimen is as effective as using a soil. Since the in-membrane test is easier to perform, less time-consuming, and more repeatable, the test is a superior alternative to the in-soil test for determining the load-deformation properties of geotextiles under typical operational conditions.

(3) The stress-confinement effect exists in the spun-bonded and needle-punched geotextiles. The stress confinement gave an

Table 5
Constants of Spun-bonded Geotextiles for Different Models up to 20% Strain Levels

Confining pressure (kgf/cm^2)	*Constants*	
(i) *Hyperbolic model*	a	b
0	18·988	0·962
0·50	9·598	0·964
0·80	5·855	1·066
(ii) *Second-order polynomial model*		
	a_1	a_2
0	$4·6 \times 10^{-2}$	$-1·0 \times 10^{-3}$
0·50	$7·5 \times 10^{-2}$	$-2·1 \times 10^{-3}$
0·80	$9·4 \times 10^{-2}$	$-5·9 \times 10^{-3}$
(iii) *Third-order polynomial model*		
	a_1	a_2 a_3
0	$5·6 \times 10^{-2}$	$-2·8 \times 10^{-3}$ $6·6 \times 10^{-5}$
0·50	$9·7 \times 10^{-2}$	$-5·9 \times 10^{-3}$ $14·2 \times 10^{-5}$
0·80	$13·4 \times 10^{-2}$	$-9·7 \times 10^{-3}$ $24·7 \times 10^{-5}$

Load per unit width in tf/m; strain as percentage.

increase in the stiffness and strength of the geotextiles. On the other hand, the heat-bonded geotextile, having a self-confined structure, had little stress-confinement effect.

(4) Representation of the load–deformation relationship of a geotextile using a hyperbolic model or a polynomial model in numerical analysis under the working stress condition requires precautions. Most of the models can only accurately simulate the behavior within a range of strain level.

The results presented in this paper were obtained from short-term tests. They implied, however, that the long-term behavior of the spun-bonded and needle-punched geotextiles under confined conditions would be different from that under unconfined conditions.

ACKNOWLEDGEMENTS

Sincere thanks are expressed to the Japanese Government for providing financial aid to the first author for his graduate study at the University of

Tokyo. The second author gratefully acknowledges the financial support of the Japanese Society for the Promotion of Science (JSPS) for his sabbatical leave at the University of Tokyo, during which this study was conducted. Mr T. Sato, technical staff of the Geotechnical Engineering Laboratory, offered his kind advice in the design of the test apparatus. Appreciations are also extended to Mitsui Petrochemicals Industries Ltd, Rhone-Poulenc Fibers, and Reemay Inc., for supplying their geotextiles. The testing apparatus was manufactured at the machine shop of the Institute of Industrial Science, University of Tokyo.

REFERENCES

Andrawes, K. Z., McGown, A., Mashhour, M. M. & Wilson-Fahmy, R. F. (1980). Tension resistant inclusions in soils. *J. Geotech. Engng, ASCE,* **106**(GT12), 1313–26.

Andrawes, K. Z., McGown, A., Wilson-Fahmy, R. F. & Mashhour, M. M. (1982). The finite element method of analysis applied to soil-geotextile systems. In *Proceedings of the Second International Conference on Geotextiles,* Las Vegas, pp. 695–700.

ASTM (1987*a*). Standard D-4632, Standard test method for breaking load and elongation of geotextiles (grab method). In *Annual Book of ASTM Standards,* Vol. 04.08. American Society for Testing and Materials, Philadelphia, pp. 1122–6.

ASTM (1987*b*). Standard D-4595, Standard test method for tensile properties of geotextiles by the wide-width strip method. In *Annual Book of ASTM Standards,* Vol. 04.08. American Society for Testing and Materials, Philadelphia, pp. 1041–55.

Chalaturnyk, R. J., Scott, J. D., Chan, D. H. K. & Richards, E. A. (1990). Stresses and deformations in a reinforced soil slope. *Can. Geotech. J.* **27,** 224–32.

Christopher, B. R., Holtz, R. D. & Bell, D. (1986). New tests for determining the in-soil stress–strain properties of geotextiles. In *Proceedings of the Third International Conference on Geotextiles,* Vienna, pp. 683–8.

El-Fermaoui, A. & Nowatzki, E. (1982). Effect of confining pressure on performance of geotextiles in soils. In *Proceedings of Second International Conference on Geotextiles,* Las Vegas, pp. 799–804.

Gray, D. H., Kaldjian, M. & Wu, C. (1989). Stress-deformation response of geotextile reinforced granular structure. In *Proceedings of Geosynthetics '89 Conference,* San Diego, pp. 373–84.

Juran, I. & Christopher, B. (1989). Laboratory model study on geosynthetic reinforced soil retaining walls. *J. Geotech. Engng, ASCE,* **115**(7), 905–26.

Kokkalis, A. & Papacharisis, N. (1989). A simple laboratory method to estimate the in-soil behavior of geotextiles. *J. Geotext. Geomembr.,* **8,** 147–57.

Konder, R. L. (1963). Hyperbolic stress–strain response: Cohesive soils. *J. Soil Mech. Foundation Division, ASCE,* **89**(1), 115–43.

Lam, W. K. & Tatsuoka, F. (1988). Triaxial compression and extension strength of sand affected by strength anisotropy and sample slenderness. In *Advanced*

Triaxial Testing of Soil and Rock, ASTM STP 977, eds R. T. Donaghe, R. C. Chaney & M. L. Silver. American Society for Testing and Materials, Philadelphia, pp. 655–66.

Li, S. Q., Lo, S. C. R. & Yu, Z. Q. (1990). Finite element study of a reinforced embankment on soft clay. In *Proceedings of the Tenth Southeast Asian Geotechnical Conference,* Taipei, pp. 77–82.

McGown, A., Andrawes, K. Z., Wilson-Fahmy, R. F. & Brady, K. C. (1981). A new method of determining the load-extension properties of geotechnical fabrics. *Transport and Road Research Laboratory Supplementary Report 704,* Berkshire, UK, 13 pp.

McGown, A., Andrawes, K. Z. & Kabir, M. H. (1982). Load-extension testing of geotextiles confined in soil. In *Proceedings of the Second International Conference on Geotextiles,* Las Vegas, pp. 793–8.

Nishigata, T. & Yamaoka, I. (1989). Tensile tests of nonwovens under confined stress. In *Proceedings of the Annual Convention of Japanese Society of Soil Mechanics and Foundation Engineering,* Tokyo, pp. 1871–2 (in Japanese).

Siel, B. D., Wu, J. T. H. & Chou, N. N. S. (1987). In-soil stress–strain behavior of geotextile. In *Proceedings of Geosynthetics '87 Conference,* New Orleans, pp. 260–5.

Tatsuoka, F. & Yamauchi, H. (1986). A reinforcing method for steep slopes using a nonwoven geotextile. *J. Geotext. Geomembr.,* **4,** 241–68.

Tatsuoka, F., Ando, H., Iwasaki, K. & Nakamura, K. (1985). Method of reinforcing cohesive embankment using a nonwoven geotextile. *Tsuchi-to-Kiso,* **33**(5), 15–20 (in Japanese).

Tatsuoka, F., Sakamoto, M., Kawamura, T. & Fukushima, S. (1986). Strength and deformation characteristics of sand in plane strain compression at extremely low pressures. *Soils and Foundations,* **26**(1), 65–84.

Wu, J. T. H. (1991). Measuring inherent load-extension properties of geotextiles for design of reinforced structures. *J. Geotech. Testing, ASTM.* Philadelphia, **14**(2), pp. 157–65.

Wu, J. T. H. & Arabian, V. (1990). Cubical and cylindrical tests for measuring in-soil load-extension properties of geotextiles. In *Proceedings of the Fourth International Conference on Geotextiles, Geomembranes and Related Products,* the Hague, p. 785.

Wu, J. T. H. & Su, C. K. (1987). Soil geotextile interaction mechanism in pullout test. In *Proceedings of Geosynthetics '87 Conference,* New Orleans, pp. 250–9.